PROCEEDINGS, 44th Workshop on Geothermal Reservoir Engineering
Stanford University, Stanford, California, February 11-13, 2019
SGP-TR-214

Microseismic Focal Mechanisms and Implications for Changes in Stress During the 2014 Newberry EGS Stimulation

Ana C. Aguiar, and Stephen C. Myers

Lawrence Livermore National Laboratory, 7000 East Ave, Livermore, CA 94550

aguiar@llnl.gov

Keywords: Microseismicity, EGS, Newberry, Focal Mechanisms, PageRank

ABSTRACT

The Newberry volcano geothermal site was stimulated to induce hydroshearing during 2012 and 2014. Aguiar and Myers (2018) relocated microseismic events for both stimulations by first using a data mining approach initially designed for webpages, Google's PageRank, to identify event clusters. They later relocated all possible events within these clusters by using a version of the Bayesloc approach (Myers *et al*., 2007) that incorporates differential arrival time data. The focus of this study is estimation of focal mechanisms for events in the 2014 relocated data set using first motion polarities of P-waves and S-waves, using the method of Shelly et al. (2016). We first manually pick P-wave and S-wave polarities for the reference event in each cluster, then use waveform cross-correlation to determine whether recordings of other events are the same or reversed polarity. We find that most events within each cluster have consistent polarities relative to the reference event, confirming the conclusion of Aguiar and Myers (2018) that events within a cluster have similar mechanisms. We also compute S/P amplitude ratios for these small events using the method of Hardebeck and Shearer (2003), and compute the mechanisms using HASH (Hardebech and Shearer, 2002), which is an open software package from the USGS that uses first motion polarities and amplitude ratios to find the best-fitting, double-couple mechanism for each event. Again, we find similar focal mechanisms within each cluster and two predominant focal mechanisms for the whole sequence. The deeper clusters have normal-fault mechanisms, whereas the shallower events, close to the top of the open hole section of the borehole, are strike-slip with east-west motion.

1. INTRODUCTION

The Newberry enhanced geothermal system (EGS), on the western flank of the Newberry Volcano in Central Oregon, was stimulated to induce hydroshearing in 2012 and 2014 by AltaRock Energy and Davenport Newberry to test and demonstrate the EGS technology (*Cladouhos et al.*, 2012). Aguiar and Myers (2018) analyzed the 2012 and 2014 sequences using a data mining technique called PageRank (*Page et al.*, 1999; *Aguiar and Beroza*, 2014) to form event clusters (families) and identify the reference event for each family that is most connected by waveform cross correlation. Differential time measurements were made for P-waves and S-waves of events within families and precise locations were determined using a modified version of Bayesloc (*Myers et al.*, 2007; 2009) that includes differential arrival time data (*Myers and Johannesson*, 2012). After relocation of the 2014 Newberry EGS events, the microseismic sequence was found to consist of six event clusters that occurred at or near contacts between lithologic units observed in the borehole (*Aguiar and Myers*, 2018) (Figure 1).

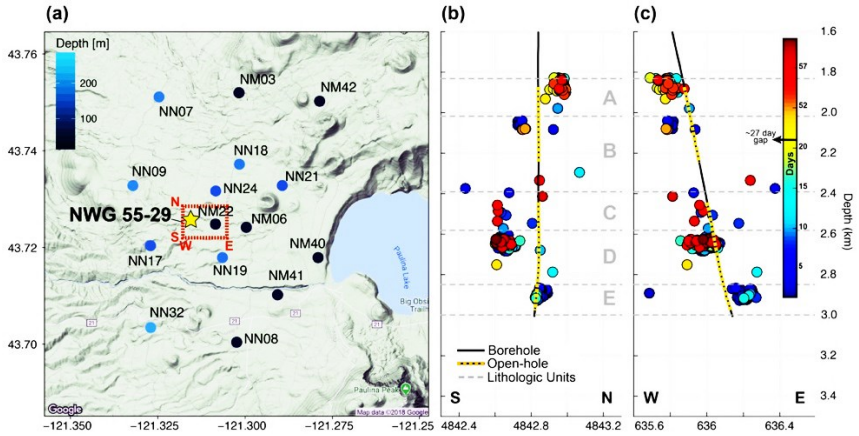

Figure 1: (a) Location map with stations used in the analysis and dashed red box showing the area in the cross sections: (b) south-north and (c) west-east. Color scale represents sequence in time for the events during the 2014 stimulation. Gray dashed lines represent lithologic units identified by Cladouhos *et al.* (2016): A-Welded lithic tuff, B-Tuff, C-Basalt basalt-andesite, D-Microcrystalline granodiorite, and E-Basalt. Black line is the borehole location and black with yellow dashed line is the open-hole section of the borehole. *Modified from Aguiar and Myers (2018).*

Precise event location provides important insights into the spatial extent of rock cracking during the stimulation. However, determining the effects of injection on the local stress field requires additional information about slip on the micro faults, which can be assessed by estimating event focal mechanisms. Determination of seismic-phase polarity, which is the most straightforward basis for determining focal mechanisms, can be challenging due to emergent phases and low signal-to-noise ratio (SNR) recordings of these small events. Fortunately, several methods have been developed to improve the robustness of focal mechanism estimates for microseismic data sets. Hardebeck and Shearer (2002; 2003) developed the HASH method that uses first-motion polarities and amplitude ratios of P-waves and S-waves to find the best fitting double-couple mechanism for each event based on a grid search. Using only first motion polarities, Shelly *et al*. (2016) showed that HASH performs well when compared to catalog mechanisms for Long Valley Caldera seismicity. Guilhem *et al*. (2014) found consistency between full moment tensor inversion solutions and HASH results for events at the Geysers geothermal field. Studies in Japan have also used HASH to estimate focal mechanisms in the Atotsugawa fault area in central Honshu (*Katsumata et al.*, 2010).

Shelly *et al*. (2016) extended focal mechanism determination for events with low SNR waveforms. They used the method of Ide *et al*. (2007) to compute the weighted, relative polarity of the low SNR waveforms with respect to the high SNR waveforms. They then applied a hierarchical clustering method to the polarity data to find groups of events with similar polarity patterns which were later used as input to HASH to determine focal mechanisms (*Shelly et al.*, 2016).

Moment tensor solutions for events associated with the 2012 and 2014 Newberry stimulations were determined using first motion polarities and amplitude ratios (*Foulger and Julian*, 2013; *Cladouhos et al.*, 2015). Results showed a wide range in focal-plane strike and a large number of moment tensor solutions with significant non-double couple components. Reported non-double couple moment tensors were particularly prominent for the small, predominantly Mw<1.3, shallower events associated with the 2014 stimulation. Cladouhos et al. (2015) suggested that these small events indicate crack-opening (*Cladouhos et al.*, 2015).

Regional stress studies based on fault mapping as well as prestimulation earthquake data suggest an east-west extensional regime and normal faulting (*Crider*, 2001; *Humphreys and Coblentz*, 2007). A similar type of faulting was observed from breakouts at the Newberry NWG-55-29 borehole utilizing a high temperature borehole televiewer before the stimulations (*Davatzes and Hickman*, 2011). These studies implied that the stress regime at Newberry is similar to the regional stresses and injection planning was based on these observations (*Cladouhos et al.*, 2015). Further analysis of moment tensors for the 2014 stimulation suggested that, as a whole, the local stress field at the time of the stimulation was not consistent with the regional stress regime, and Cladouhos *et al*. (2015) speculate that the stress field at the bottom of the well might be dependent on other factors, such as the location of the Newberry magma chamber. Even thought the size of the magma chamber is not well constrained, calculations for different depths suggest that stress due to the magma chamber might be substantial, with a horizontal E-W compression as the strongest stress (*Cladouhos et al.*, 2015). Overall, however, there is no clear pattern in the moment tensors analyzed by Cladouhos *et al*. (2015) and no consistency between events at similar depths, so the microseismic moment tensors infer an extremely complicated stress field.

Fluid injection in 2012 breached the shallow borehole casing, resulting in most microseismic activity occurring shallower than the target region. After repair of the casing, the 2014 stimulation generated microseismic events in the target region (*Cladouhos et al.*, 2016), so we focus this study on analysis of the 2014 events. Event locations presented in Aguiar and Myers (2018) for the 2014 sequence are different enough from the locations used for previous moment tensor and focal mechanism studies that ray take off angles are effected. Aguiar and Myers (2018) also find that events are far more clustered than previous studies suggest and waveforms within clusters are similar, suggesting similar focal mechanisms. New location results and observations of waveform similarity prompt a new evaluation of Newberry focal mechanisms.

2. FOCAL MECHANISMS ESTIMATION

We generally follow the method of Shelly *et al*. (2016) to determine focal mechanisms for the 2014 microseismic sequence at the Newberry EGS with a few modifications that leverage the measurements and results of Aguiar and Myers (2018). With waveform cross correlations already computed and event clusters identified, we start the focal mechanism analysis at the polarity measurement stage of the process. Further, we can utilize the phase-windowed correlation results to determine P-waves and S-waves polarity independently, which is a significant refinement to using long windows that may contain both phases (*Shelly et al.*, 2016). We also rotate the data to the principal direction of motion (explained below) whereas Shelly *et al*. (2016) uses a three-component correlation approach.

Aguiar and Myers (2018) identified 6 main clusters in the 2014 data set, 4 of which meet data coverage criteria (specified below) for focal mechanism analysis. We start the analysis by applying a 5-10 Hz bandpass filter, which significantly increases SNR. We then rotate the three component seismograms to maximize P-wave and S-wave amplitudes. First, the P-wave window is rotated to the principle eigen vector of particle motion. Second, the S-wave window is rotated to the principle eigen vector under the constraint that particle motion is perpendicular to the P-wave. We use the rotated data set to manually pick P-wave and S-wave polarities for the reference event in each event cluster. Relative polarities for other events in the cluster are determined with respect to the reference event by testing whether normal or reversed-polarity seismograms have a higher correlation coefficient (*Shelly et al.*, 2016).

After polarity information was recorded, we computed the S/P amplitude ratios for all stations with clear polarities and used these measurements as input to HASH (*Hardebeck and Shearer*, 2003) to constrain the focal mechanisms. We only included events that have polarity information at a minimum of 5 stations spanning 4 azimuthal quadrants. This eliminates 56 of the 209 relocated events from the 2014 data set, leaving 153 events in the sequence for the HASH analysis. Processing for each of the 4 event clusters was done

independently. We used a 1D velocity gradient model to determine ray takeoff, because there is little difference in takeoff angles for the Newberry data set when using a simple 1D velocity gradient model versus the 3D velocity model from Matzel *et al*. (2014).

3. RESULTS AND INTERPRETATION

After analyzing all 4 clusters of the 2014 data set independently, we found two stations (NM03 and NN17) with a significant number of clear polarity reversals. All the reversals were associated with events in the largest cluster in the analysis, which is associated to reference event 82. We separated this cluster into two subsets of events, each with distinct waveform polarity. Events with reversed seismograms with respect to the reference event occur throughout the duration of the sequence, suggesting that polarity reversal is not the result of a change in instrumentation setting.

The few phase polarity reversals notwithstanding, focal mechanisms for events in each cluster are similar (Figure 2). We identify a single type of focal mechanism for all events in the clusters associated with reference events 77, 227, and 298. Focal mechanisms for events associated with reference event 82 have similar normal fault mechanisms, but as mentioned 2 distinct sub-clusters are distinguished by a slight difference in fault-plane strike (Figure 2b). The first subgroup (Ev82 – G1 in Figure 2) has the same polarity seismograms at all stations as the reference event. Seismograms recorded on NM03 and NN17 are reversed for the second subgroup (Ev82 – G2 in Figure 2). This is also the group with the highest variability in fault-plane strike.

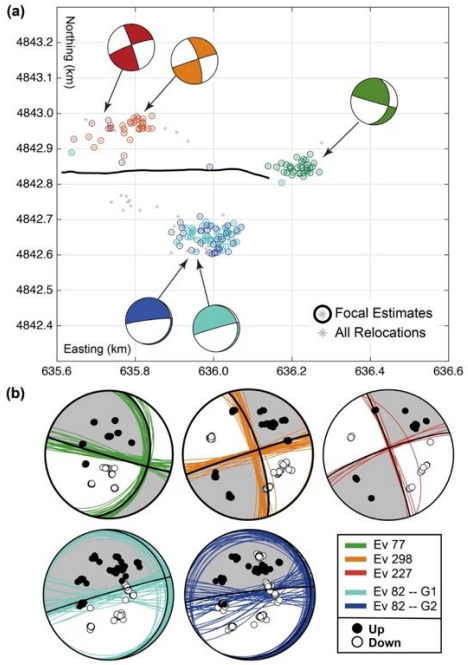

Figure 2: (a) Map view of locations for the 2014 relocated microseismic events color coded by focal mechanism grouping. Gray stars represent events for which focal mechanism solutions could not be robustly determined. (b) Black focal planes with grey-shaded compressional regions are the median focal mechanisms for each group. Color focal planes for each event comprising the group show the variability within each group. Filled and open dots are lower-hemisphere projections of compressional and dilatational P-wave rays, respectively.

One focal plane for each event group aligns with the map-view trend for event locations determined by Aguiar and Myers (2018). Further, event locations migrate away from the borehole with time along these trends, suggesting that the trends are not due to event location uncertainty, i.e. the trend is not caused by multiple realizations drawn from a common spatial probability density function (e.g. uncertainty ellipsoid). These results give us confidence that the focal plane aligning with event locations is the fault plane, and the other focal plane is the auxiliary plane that indicates slip direction. The sense of motion on the steep fault planes is shown as dashed black-arrowed lines in Figure 3, and the style of faulting is distinctly different for the shallow and deep clusters. Right-lateral, strike-slip events comprise the shallow clusters, and steeply dipping north-down, normal-fault events comprise the two deeper clusters (Figure 3c).

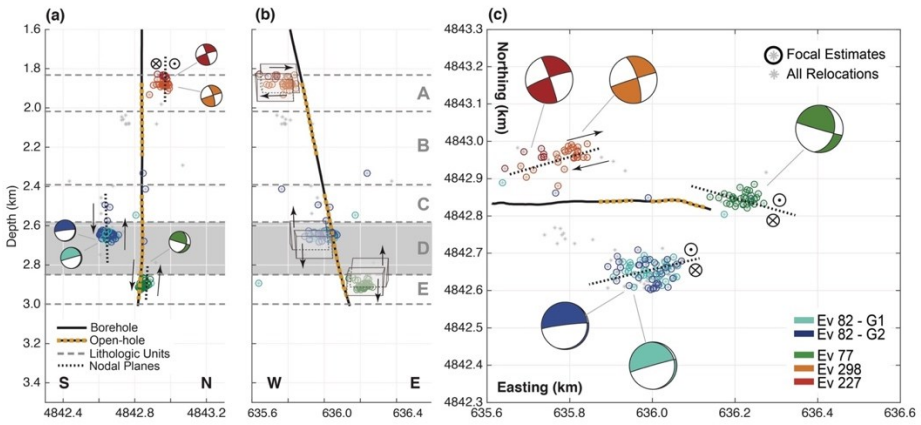

Figure 3: Cross-sections and map view of 2014 Newberry locations and color-coded by focal mechanism type. Cross sections are (a) South to North and (b) West to East. (c) Map view. Dashed black lines are interpreted fault planes and arrowed lines show direction of motion on the faults. Gray dashed lines are the same lithologic units listed in the Figure 1 caption (A-E). Black solid line is the borehole location and black and yellow dashed line is the open-hole section of the borehole.

4. DISCUSSION

The focal mechanism solutions and event locations reported by Aguiar and Myers (2018) can be explained by stress related to fluid injection radiating outward from the open-hole portion of the injection well, which is consistent with modeling studies (e.g. *Kim and Hosseini*, 2017).

Events of Mw > 4 near the Newberry EGS are mostly normal fault events. Regional stress analysis based on these events suggest that the least compressive stress (S_{hmin}) is oriented approximately E-W, the intermediate stress (S_{Hmax}) is approximately N-S and the greatest compressive stress is near vertical (*Crider*, 2001). Fracture measurements using a borehole televiewer at Newberry well 55-29 were made in October of 2010, before either stimulation. Borehole breakouts suggest similar stress directions for S_{Hmax} and S_{hmin} as the regional field. Assuming that the maximum principal stress is vertical (S_v), the borehole breakout is also indicative of normal faulting with a N-S trending strike (*Cladouhos et al.*, 2011; *Davatzes and Hickman*, 2011; *Cladouhos et al.*, 2016).

We find that normal faulting is predominant below ~2.6 km depth during the stimulation, but the focal mechanisms suggest that the directions of S_{Hmax} and S_{hmin} are rotated 90° compared to regional studies and measurements in the borehole before the hydroshear stimulation. Shallower focal mechanisms are consistent with S_{Hmax} and S_{hmin} directions that align with the regional stress, but the strike-slip mechanism suggests that the maximum principal stress is horizontal, instead of vertical. A possible explanation for the deep focal mechanisms is that the pressure produced by fluid injection caused increased horizontal stress that was not sufficient to overcome vertical loading, but resulted in a ~90° rotation of the stress field around a vertical axis. Whereas, in the shallower portion of the borehole, fluid injection increased horizontal stress to the point where horizontal stress became the dominant stress direction, i.e. rotation of the stress field around a horizontal axis. Given that pre-stimulation values for S_{Hmax} and S_v computed for the the Newberry site are similar for shallower depths (S_{Hmax} ~ 94% of S_v at ~ 1.9 km) and the difference between these values increases with depth (S_{Hmax} ~ 86% of S_v at ~ 2.6 km) (*Davatzes and Hickman*, 2011; *Cladouhos et al.*, 2016), it is plausible that an increase in pressure during stimulation would cause S_{Hmax} to exceed S_v at shallower depths but not at greater depth. Similar changes in fault type with depth have also been reported at the Geysers, where shallower events are strike-slip and deeper events are normal faults, with evidence of some transtensional behavior in between (*Martínez-Garzón et al.*, 2013).

In general, modeling of spatio-temporal variations in stress within and around a stimulated volume show that the variation in focal mechanisms that we observe are consistent with changes in stress generated by fluid injection and production (*Segall and Fitzgerald*, 1998). More recent studies focused on a variety of study areas have reported that total stresses can change with changes in pore pressure (*Kim and Hosseini*, 2017). A global average shows that the change in horizontal stress can be about 2/3 of the change in pore pressure (*Hillis*, 2000; *Altmann et al.*, 2010), but within the injection zone the ratio of the change in vertical stress and change in pore pressure can be close to zero (*Kim and Hosseini*, 2017). Predictions of increased horizontal stress and little change in vertical stress are consistent with the stress field inferred by the Newberry microseismicity at the time of the 2014 stimulation. Also, the pressure needed to induce hydroshearing at Newberry was much greater than originally thought, with hydroshearing starting at 180 bar (18 MPa) instead of the 93 bar (9.3 MPa) computed from initial modeling (*Cladouhos et al.*, 2015). Both the tendency for fluid pressure to influence horizontal stress more than vertical stress and the high fluid pressure reported at Newbery support an interpretation of S_{Hmax} changing enough to surpass the value of S_v at shallower depths. Our observations also suggest that at greater depths, the injection pressures worked against the regional stress field, and cracks did not slip until overcoming and rotating the ambient, horizontal stress field. This could be a potential explanation for why the fracture network generated by the stimulation was limited, and the flow to the borehole did not increase significantly after the stimulation.

We note that the HASH method is limited to purely double-couple solutions, and previous studies report moment-tensor solutions with non-double couple components for the Newberry 2014 events (*Cladouhos et al.*, 2015). Further, none double-couple moment tensors, opening/closing cracks, are reported in other geothermal environments (*Miller et al.*, 1998; *Ross et al.*, 1999; *Dreger et al.*, 2000; *Julian and Foulger*, 2004). In an effort to compare results, we found that only 30% of events in our analysis overlap with events for which moment tensors have been determined, so a comprehensive comparison would not be conclusive. However, the general sense of motion prescribed by the moment tensor solutions (*Cladouhos et al.*, 2015) agrees with our results, i.e. north down motion at depth and right lateral for shallower events. Regardless, the inferred opening of cracks implied by the small number of non-double component in Newberry moment tensors does not change our conclusions.

4. CONCLUSIONS

Utilizing the methods of Shelly et al. (2016) and Hardebeck and Shearer (2003) we show that the same waveform cross-correlation results that are used in the PageRank method (*Aguiar and Beroza*, 2014; *Aguiar and Myers*, 2018) can also aid in the determination of focal mechanisms generated by the 2014 Newberry EGS stimulation. We utilize the results of the relocation study by Aguiar and Myers (2018) that clustered the events and improved the estimates of ray takeoff angles to compute focal mechanisms for this event sequence. In contrast to previous studies, we find consistent source types for each of the clusters analyzed, with some variability in the strike of the fault plane in the largest cluster. The results demonstrate that the focal mechanism for the cluster reference event is generally representative of the focal mechanism for all events in the cluster, affirming that PageRank links events with similar physical properties, e.g. location and focal mechanism.

The deeper events are normal faults, but the inferred stress orientation is rotated 90° around a vertical axis with respect to the stress field determined in regional studies. The shallow events are strike-slip faults, and the direction of inferred horizontal stresses are consistent with the regional principal stress directions. However, the maximum principal stress inferred by the shallow events is horizontal, in contrast to the vertical maximum stress inferred by regional studies. Fluid injection increased horizontal stress beyond the vertical stress imposed by the overburden in the shallower portions of the EGS, resulting in rotation of the maximum compressive stress from vertical to horizontal. Our focal mechanism results are consistent with numerical modeling of fluid injection suggesting that increases in horizontal stress can be 2/3 the increase in fluid pressure, whereas the increases in vertical stress can be near zero. The location and orientation of observed faulting with respect to the injection borehole suggest that fluid injection pressures worked against the regional stress field, which may explain why the spatial extent of micro-seismic activity was limited and fluid flow after the stimulation did not increase as much as expected.

This work was performed under the auspices of the U.S. Department of Energy by Lawrence Livermore National Laboratory under Contract DE-AC52- 07NA27344. LLNL-PROC-767066

REFERENCES

Aguiar, A. C., and G. C. Beroza (2014), PageRank for Earthquakes, *Seismological Research Letters* **85**, 2, doi:10.1785/0220130162.

Aguiar, A. C., and S. C. Myers (2018), Microseismic Event Relocation Based on PageRank Linkage at the Newberry Volcano Geothermal Site, *Bulletin of the Seismological Society of America* doi:10.1785/0120180115.

Altmann, J. B., T. M. Müller, B. I. R. Müller, M. R. P. Tingay, and O. Heidbach (2010), Poroelastic contribution to the reservoir stress path, *International Journal of Rock Mechanics and Mining Sciences* **47**, 7, doi:10.1016/j.ijrmms.2010.08.001.

Cladouhos, T. T. et al. (2015), Newberry EGS Demonstration: Phase 2.2 Report, doi:10.2172/1214834.

Cladouhos, T. T., S. Petty, M. W. Swyer, M. E. Uddenberg, K. Grasso, and Y. Nordin (2016), Results from Newberry Volcano EGS Demonstration, 2010–2014, *Geothermics* **63**, doi:10.1016/j.geothermics.2015.08.009.

Cladouhos, T. T., S. Petty, O. Callahan, W. Osborn, S. Hickman, and N. Davatzes (2011), The role of stress modeling in stimulation planning at the Newberry Volcano EGS Demonstration Project, *Proceedings of the 36th Workshop on Geothermal Reservoir Engineering*, Stanford University, Stanford, California, SGP-TR-191.

Cladouhos, T. T., W. L. Osborn, S. Petty, D. Bour, J. Lovennitti, O. Callahan, Y. Nordin, D. Perry, and P. L. Stern (2012), Newberry volcano EGS demonstration–phase I results, *Proceedings of the 37th Workshop on Geothermal Reservoir Engineering*, Stanford University, Stanford, California, SGP-TR-194.

Crider, J. G. (2001), Oblique slip and the geometry of normal-fault linkage: mechanics and a case study from the Basin and Range in Oregon, *Journal of Structural Geology* **23**, 12, doi:10.1016/S0191-8141(01)00047-5.

Davatzes, N. C., and S. H. Hickman (2011), Preliminary Analysis of Stress in the Newberry EGS Well NWG 55-29, *GRC Trans* **35**, p. 323-332.

Dreger, D. S., H. Tkalčić, and M. Johnston (2000), Dilational Processes Accompanying Earthquakes in the Long Valley Caldera, *Science* **288**, 5463, doi:10.1126/science.288.5463.122.

Foulger, G. R., and B. R. Julian (2013), Micro-earthquake technology for EGS fracture characterization, *Final Report* doi:10.2172/1248498.

Guilhem, A., L. Hutchings, D. S. Dreger, and L. R. Johnson (2014), Moment tensor inversions of M ~ 3 earthquakes in the Geysers geothermal fields, California, *Journal of Geophysical Research: Solid Earth* **119**, 3, doi:10.1002/2013JB010271.

Hardebeck, J. L., and P. M. Shearer (2002), A New Method for Determining First-Motion Focal Mechanisms, *Bulletin of the Seismological Society of America* **92**, 6, doi:10.1785/0120010200.

Hardebeck, J. L., and P. M. Shearer (2003), Using S/P Amplitude Ratios to Constrain the Focal Mechanisms of Small Earthquakes, *Bulletin of the Seismological Society of America* **93**, 6, doi:10.1785/0120020236.

Hillis, R. (2000), Pore Pressure/Stress Coupling and its Implications for Seismicity, *Exploration Geophysics* **31**, 1-2, doi:10.1071/EG00448.

Humphreys, E. D., and D. D. Coblentz (2007), North American dynamics and western U.S. tectonics, *Rev. Geophys.* **45**, RG3001, doi:10.1029/2005RG000181.

Ide, S., D. R. Shelly, and G. C. Beroza (2007), Mechanism of deep low frequency earthquakes: Further evidence that deep non-volcanic tremor is generated by shear slip on the plate interface, *Geophys. Res. Lett.* **34**, 3, doi:10.1029/2006GL028890.

Julian, B. R., and G. R. Foulger (2004), Microearthquake Focal Mechanisms, A Tool for Monitoring Geothermal Systems, *GRC Bulletin*, July/August 2004.

Katsumata, K., M. Kosuga, H. Katao, Japanese University Group of the Joint Seismic Observations at NKTZ (2010), Focal mechanisms and stress field in the Atotsugawa fault area, central Honshu, Japan, *Earth Planet Sp* **62**, 4, doi:10.5047/eps.2009.12.006.

Kim, S., and S. A. Hosseini (2017), Study on the ratio of pore-pressure/stress changes during fluid injection and its implications for CO2 geologic storage, *Journal of Petroleum Science and Engineering* **149**, doi:10.1016/j.petrol.2016.10.037.

Martínez-Garzón, P., M. Bohnhoff, G. Kwiatek, and G. Dresen (2013), Stress tensor changes related to fluid injection at The Geysers geothermal field, California, *Geophys. Res. Lett.* **40**, 11, doi:10.1002/grl.50438.

Matzel, E., D. Templeton, A. Petersson, and M. Goebel (2014), Imaging the Newberry EGS site using seismic interferometry, *Proceedings of the 39th Workshop on Geothermal Reservoir Engineering*, Stanford University, Stanford, California, SGP-TR-202.

Miller, A. D., G. R. Foulger, and B. R. Julian (1998), Non-double-couple earthquakes 2. Observations, *Rev. Geophys.* **36**, 4, doi:10.1029/98RG00717.

Myers, S. C., and G. Johannesson (2012), Extension of the Bayesloc Multiple-Event Location Algorithm to Include Differential Travel Time Measurements, *Proceedings of the Monitoring Research Review Ground-Based Nuclear Explosion Monitoring Technologies* **1**.

Myers, S. C., G. Johannesson, and W. Hanley (2007), A Bayesian hierarchical method for multiple-event seismic location, *Geophys. J. Int.* **171**, 3, doi:10.1111/j.1365-246X.2007.03555.x.

Myers, S. C., G. Johannesson, and W. Hanley (2009), Incorporation of probabilistic seismic phase labels into a Bayesian multiple-event seismic locator, *Geophys. J. Int.* **177**, 1, doi:10.1111/j.1365-246X.2008.04070.x.

Page, L., S. Brin, R. Motwani, and T. Winograd (1999), The PageRank Citation Ranking: Bringing Order to the Web, *Technical Report*, Stanford InfoLab.

Ross, A., G. R. Foulger, and B. R. Julian (1999), Source processes of industrially-induced earthquakes at The Geysers geothermal area, California, *Geophysics* **64**, 6, doi:10.1190/1.1444694.

Segall, P., and S. D. Fitzgerald (1998), A note on induced stress changes in hydrocarbon and geothermal reservoirs, *Tectonophysics* **289**, doi:10.1016/S0040-1951(97)00311-9.

Shelly, D. R., J. L. Hardebeck, W. L. Ellsworth, and D. P. Hill (2016), A new strategy for earthquake focal mechanisms using waveform-correlation-derived relative polarities and cluster analysis: Application to the 2014 Long Valley Caldera earthquake swarm, *Journal of Geophysical Research: Solid Earth* **121**, 12, doi:10.1002/2016JB013437.